

Super-resolution filtered ghost imaging with compressed sensing

Shao-Ying Meng(孟少英), Wei-Wei Shi(史伟伟), Jie Ji(季杰), Jun-Jie Tao(陶俊杰), Qian Fu(付强), Xi-Hao Chen(陈希浩), and Ling-An Wu(吴令安)

Citation: Chin. Phys. B, 2020, 29 (**12**): 128704. DOI: 10.1088/1674-1056/abc15f
Journal homepage: http://cpb.iphy.ac.cn; http://iopscience.iop.org/cpb

What follows is a list of articles you may be interested in

The determinant factors for map resolutions obtained using CryoEM single particle imaging method

Yihua Wang(王义华), Daqi Yu(余大启), Qi Ouyang(欧阳颀), Haiguang Liu(刘海广)
Chin. Phys. B, 2018, 27 (**12**): 128702. DOI: 10.1088/1674-1056/27/12/128702

Applications of nanostructures in wide-field, label-free super resolution microscopy

Xiaowei Liu(刘小威), Chao Meng(孟超), Xuechu Xu(徐雪初), Mingwei Tang(汤明炜), Chenlei Pang(庞陈雷), Qing Yang(杨青)
Chin. Phys. B, 2018, 27 (**11**): 118704. DOI: 10.1088/1674-1056/27/11/118704

Novel Fourier-based iterative reconstruction for sparse fan projection using alternating direction total variation minimization

Zhao Jin(金朝), Han-Ming Zhang(张瀚铭), Bin Yan(闫镔), Lei Li(李磊), Lin-Yuan Wang(王林元), Ai-Long Cai(蔡爱龙)
Chin. Phys. B, 2016, 25 (**3**): 038701. DOI: 10.1088/1674-1056/25/3/038701

RAPID COMMUNICATION

Super-resolution filtered ghost imaging with compressed sensing*

Shao-Ying Meng(孟少英)[1], Wei-Wei Shi(史伟伟)[1], Jie Ji(季杰)[1], Jun-Jie Tao(陶俊杰)[1], Qian Fu(付强)[1], Xi-Hao Chen(陈希浩)[1,†], and Ling-An Wu(吴令安)[2]

[1] *Key Laboratory of Optoelectronic Devices and Detection Technology, School of Physics, Liaoning University, Shenyang* 110036, *China*
[2] *Institute of Physics, Chinese Academy of Sciences, Beijing* 100190, *China*

(Received 17 August 2020; revised manuscript received 22 September 2020; accepted manuscript online 15 October 2020)

A filtered ghost imaging (GI) protocol is proposed that enables the Rayleigh diffraction limit to be exceeded in an intensity correlation system; a super-resolution reconstructed image is achieved by low-pass filtering of the measured intensities. In a lensless GI experiment performed with spatial bandpass filtering, the spatial resolution can exceed the Rayleigh diffraction bound by more than a factor of 10. The resolution depends on the bandwidth of the filter, and the relationship between the two is investigated and discussed. In combination with compressed sensing programming, not only high resolution can be maintained but also image quality can be improved, while a much lower sampling number is sufficient.

Keywords: ghost imaging, bandpass filtering, compressed sensing, super resolution

PACS: 87.57.cf, 87.63.lm **DOI:** 10.1088/1674-1056/abc15f

1. Introduction

The resolution bound of various optical imaging systems is one of the most important issues in both science and engineering, and is well known as the Abbe–Rayleigh criterion.[1] Researchers have attempted to overcome this limitation and to understand its fundamental implications for centuries. Recently, great breakthroughs have been achieved in biological microscopic imaging, and a new generation of super-resolution microscopy can exceed the Rayleigh diffraction limit.[2–4] Besides these traditional lens imaging systems, a newly-developed ghost imaging (GI) scheme[5–13] is a potential candidate for super-resolution imaging in systems both with and without lenses.[14–20] After more than ten years' development, thermal GI has gradually overcome its drawbacks of low visibility, low signal-to-noise ratio, and long integration time by various schemes such as high-order GI,[21–23] differential GI,[24] computational GI,[25] correspondence imaging,[26] and compressed GI,[27] while its ability to break the diffraction barrier and achieve a super-resolution image has been verified in various recent schemes.[16–20]

Recently, we proposed a new approach for reconstructing super-resolution images of objects in a lensless low-pass filtered GI (FGI) system at a resolution greatly exceeding the Rayleigh diffraction bound defined by the numerical aperture of the system, where the spatial resolution can be improved by more than a factor of 2.[19,20] The anti-correlation effect of optical intensities was also observed via manipulating the filtering thresholds in a two-arm optical setup.[20] As the intensity of each random speckle has a Gaussian distribution, spatial bandpass filtering will result in a hollow or doughnut shaped intensity distribution. The essence of our method is that we selectively filter the intensity of each random laser speckle in the detection plane by digital processing. It should be emphasized that in our FGI scheme filtering is performed in the spatial and not the frequency domain.[15,28] The function of our filtering is somewhat similar to the formation of the hollow planar intensity distribution of the obstructed condenser lens in a macroscopic system,[29] as well as the so-called 'doughnuts' intensity pattern in a nanoscopic system,[30] and the hollow Bessel beam in stimulated emission depletion microscopy.[31] All the above methods aim at removing or obstructing the central parts of the intensity distribution; the difference is that the latter create hollow intensity patterns while we selectively filter the spatial intensity distribution by digital processing. Although it was shown that FGI can enhance the resolution by a factor of more than 2,[19,20] there are still various unsolved issues that required further consideration. One of the most important questions is, what is the actual limit to the super-resolution in FGI, or to what extent can it exceed the diffraction limit?

To address some of the above issues, in this paper we demonstrate experimentally that, through spatial bandpass filtering of the instantaneous intensities, FGI in a lensless optical setup can achieve a super-resolution that exceeds the Rayleigh diffraction limit by more than a factor of 10. This factor could be even greater with further optimization of the optics. By combining with compressed sensing (CS), the sampling number can be reduced to less than 10% of the Nyquist limit with-

*Project supported by the National Key Research and Development Program of China (Grant Nos. 2018YFB0504302 and 2017YFB0503301) and Defense Industrial Technology Development Program (Grant No. D040301-1).

†Corresponding author. E-mail: xi-haochen@163.com

© 2020 Chinese Physical Society and IOP Publishing Ltd

out affecting the image quality and high resolution. It is also observed that FGI, not CS, plays the key role in the improvement of the resolution.

2. Theory and method

The experimental setup is depicted in Fig. 1, which is the same as the FGI system that we previously reported.[19,20] Here for convenience and without loss of generality, in the following theoretical section we only consider the intensity along the horizontal direction. If both the spatial filters TFi $(i=1,2)$ are removed, the setup will become a traditional Hanbury Brown and Twiss (HBT) system. The corresponding normalized second-order intensity correlation function with thermal light in the detection plane will be represented by

$$g^{(2)}(x_1,x_2)=\frac{\langle I(x_1)I(x_2)\rangle}{\langle I(x_1)\rangle\langle I(x_2)\rangle}, \tag{1}$$

where $I(x_i)$ $(i=1,2)$ are the intensity distributions of the fields at distances x_1, x_2 on the X_1, X_2 planes, and the distances z_1, z_2 from the light source to the CCD planes X_1, X_2, respectively, are equal. When an object is inserted before CCD1, which we take to be the bucket detector, the corresponding ghost image in a traditional GI system is given by

$$g^{(2)}(x_2)=\frac{\langle SI(x_2)\rangle}{\langle S\rangle\langle I(x_2)\rangle}, \tag{2}$$

where $S=\int I(x_1)\mathrm{d}x_1$ is the total integrated intensity collected by CCD1.

However, if two spatial filters TF1 and TF2 are inserted into their respective beams behind the spatially resolving detectors CCD1 and CCD2 before connection to the coincidence circuit, the instantaneous intensity distributions that are actually measured after filtering are modified as $I_{B1}(x_1)$ and $I_{B2}(x_2)$, where $B_i=T_i'-T_i+1$ $(i=1,2)$ are the bandwidths of the filters, respectively, while T_i $(i=1,2)$ and T_i' $(i=1,2)$ are the lower and upper bounds of the bandwidth B_i. Then, the normalized second-order intensity correlation function after bandpass filtering becomes

$$g_B^{(2)}(x_1,x_2)=\frac{\langle I_{B1}(x_1)I_{B2}(x_2)\rangle}{\langle I_{B1}(x_1)\rangle\langle I_{B2}(x_2)\rangle}. \tag{3}$$

If CCD1 and TF1 in the object arm play the usual role of a GI bucket detector, i.e., $S_{B1}=\int I_{B1}(x_1)\,\mathrm{d}x_1$, then the ghost image reconstructed with $I_{B2}(x_2)$ from the normalized second-order intensity correlation function can be rewritten as

$$g_B^{(2)}(x_2)=\frac{\langle S_{B1}I_{B2}(x_2)\rangle}{\langle S_{B1}\rangle\langle I_{B2}(x_2)\rangle}. \tag{4}$$

It should be emphasized that the distances z_1 and z_2 from the thermal source to the object and CCD2 must be equal for lensless GI.

Whether in traditional GI or FGI, the necessity of taking a sufficiently large number of exposures is always an obstacle in reconstructing real-time images, and costs a lot of time in data capture and calculation, thus limiting practical applications. Moreover, due to the statistical nature of GI there seems to be little advantage in image quality compared to traditional lens imaging, even though many attempts at improvement have been made. Fortunately, with the introduction of compressed sensing the number of samples required can be reduced to less than 5% of the Nyquist limit while at the same time the image quality can be greatly enhanced compared with ordinary GI.[32] We shall show here that FGI combined with CS can reconstruct images with not only super-resolution but also excellent image quality and much smaller sampling number.

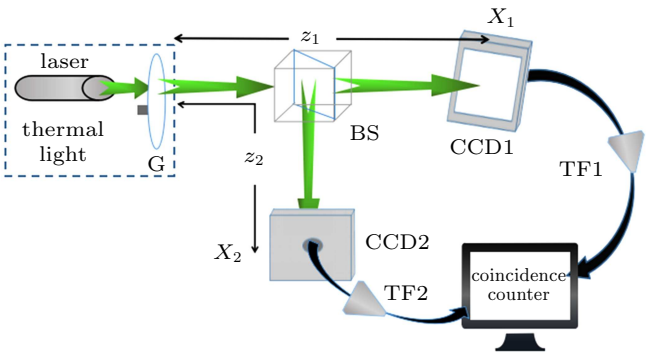


Fig. 1. Schematic of experimental setup. G, ground-glass plate; BS, beamsplitter; CCD1 and CCD2, spatially resolving cameras; TF1 and TF2; spatial bandpass filters; z_1 and z_2, distances from the thermal source to the object plane X_1 and CCD2 plane X_2, respectively.

In the CS framework,[16,27,28,33,34] for the GI/FGI system shown in Fig. 1, the intensity distribution $I(x_2)$ $(I_{B2}(x_2))$ in the reference arm at a certain time is usually reshaped as a row vector $(1\times n, n=N\times M)$, which is a captured frame with a size of $N\times M$ pixels in a practical measurement. For the k captured frames, a $k\times n$ matrix $\boldsymbol{A}$ will be constructed while the bucket intensities $S(S_{B1})$ in the test arm will be transformed into a column vector $\boldsymbol{y}(k\times 1)$. If we denote an unknown object inserted before CCD1 in Fig. 1 as an N-dimensional vector $\boldsymbol{x}$ and there exists a transform operator $\boldsymbol{\psi}$ in the sparse basis that satisfies $\boldsymbol{x}=\boldsymbol{\psi}\cdot\boldsymbol{x}'$, where $\boldsymbol{x}'$ is sparse in the presentation basis $\boldsymbol{\psi}$, then the image can be recovered by solving the following convex optimization problem:

$$\boldsymbol{x}=\boldsymbol{\psi}\cdot\boldsymbol{x}', \text{ which minimizes } \frac{1}{2}\|\boldsymbol{A}\boldsymbol{x}-\boldsymbol{y}\|_2^2+\tau\|\boldsymbol{x}'\|_1. \tag{5}$$

Here, τ is a nonnegative parameter, $\|\boldsymbol{V}\|_2$ denotes the Euclidean norm of $\boldsymbol{V}$, and $\|\boldsymbol{V}\|_1=\sum_i|v_i|$ is the l_1 norm of $\boldsymbol{V}$. It is quite general to permit the apriori assumption that an object can be sparsely expressed in a known basis, because many natural objects are indeed sparse in an appropriate basis. As described in previous studies, the main characteristic of CS is that it can be utilized to find the sparsest solution of a set of

equations to achieve an improved quality image of an object within shorter acquisition time.

3. Experiments and results

The setup shown in Fig. 1 is a generic FGI system employing classical thermal light, and the experimental procedure of filtering is basically the same as that in our previous papers.[19,20] A laser beam of wavelength $\lambda = 532$ nm and beam diameter $D = 3$ mm illuminates a rotating ground-glass plate G to generate pseudothermal light. The scattered beam is divided by a 50 : 50 nonpolarizing beamsplitter (BS) into two beams; one beam is transmitted into the test arm and the other is reflected into the reference arm, to be detected by cameras CCD1 and CCD2 (Imaging Source DMK), respectively. The data from each detector is saved to a computer, and then filtering of the intensity distributions is performed by means of data processing through matrix manipulation in Matlab. The actual operations are as follows: Firstly, we choose two different numbers T_i and T_i' $(T_i < T_i')$ as the lower bound and upper bound, respectively. Their difference plus 1, i.e., $T_i' - T_i + 1$, is the bandwidth B_i. Secondly, each instantaneous intensity value of the thermal light in a plane is compared with given lower and upper bounds; if this value is lower than the lower bound or larger than the upper bound, it will be set to 0; if it is smaller than or equal to the upper bound and larger than or equal to the lower bound, it will not be changed. Finally, the filtered data are used to calculate the second-order correlation functions as in traditional GI. The parameters of the bandpass filters are of course crucial, and will be discussed in detail in this paper. All the images are retrieved after averaging over a series of exposure frames.

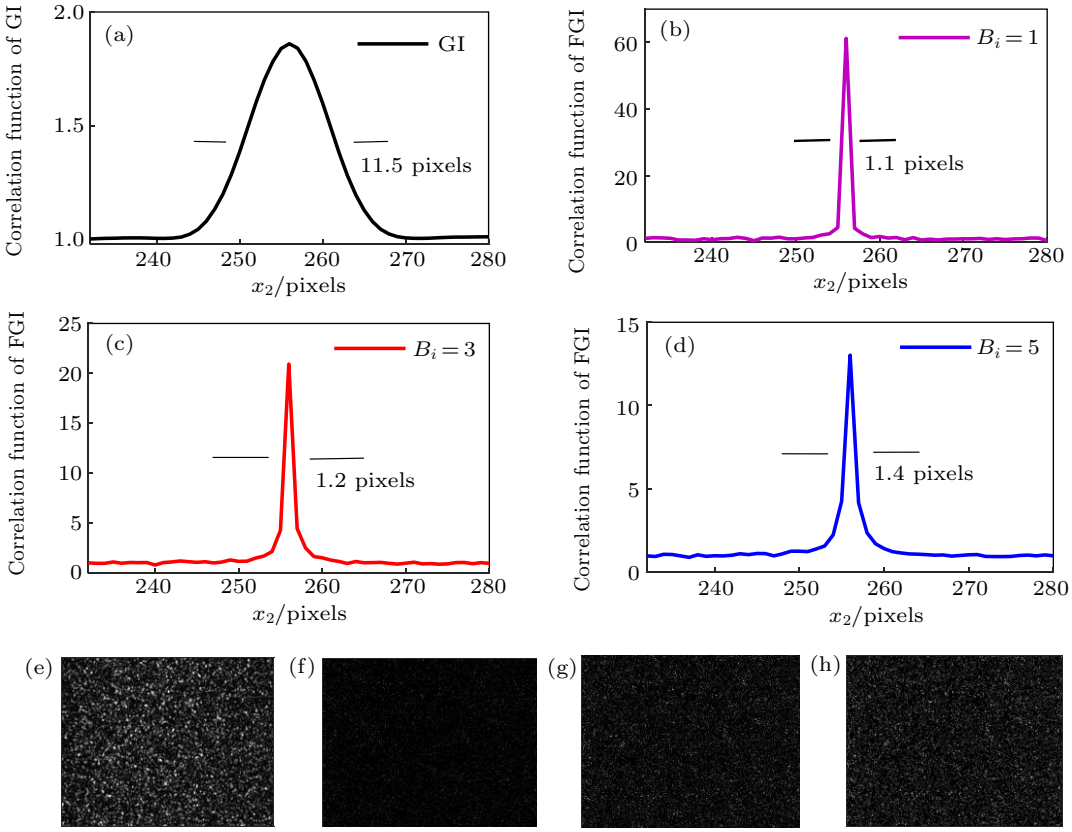


Fig. 2. HBT spatial resolution in traditional GI (a), and in FGI for bandwidths of (b) $B_i = 1$, (c) $B_i = 3$, (d) $B_i = 5$. (e) A randomly chosen speckle pattern for GI, and (f)–(h) its filtered speckle patterns after filtering with bandwidths of 1, 3, and 5, from which (b)–(d) were plotted, respectively.

It is well-known that the transverse spatial resolution in a lensless GI system is usually defined as the full-width at half-maximum (FWHM) of a spatial HBT-type intensity correlation function under the same experimental conditions. To determine how much the resolution can be improved by our FGI method, we first measure the spatial HBT coincidence functions to estimate the resolution of the imaging system by using both traditional GI and bandpass FGI. The resolutions for the different bandwidths are obtained by calculating the corresponding FWHMs of the 2nd-order autocorrelation functions of the intensity distributions $I(x_1)$ and $I_{B1}(x_1)$ with respect to Eqs. (1) and (3), respectively, as in our previous paper.[19] The results are shown in Fig. 2. Figures 2(e)–2(h) show a randomly chosen pattern (e) which was then filtered with a bandwidth of $B_i = 1$, 3, and 5 and used to plot the HBT peaks in Figs. 2(b)–2(d), respectively. From Fig. 2(a) we see that the resolution is about 11.5 pixels in the traditional GI setup, while for FGI the resolutions are about 1.1, 1.2, and 1.4 pixels for the band-

widths of $B_i = 1$, 3, and 5, respectively. It is evident that the resolution can be as fine as 1.1 pixels in FGI, which corresponds to an enhancement of more than a factor of 10, i.e., an order of magnitude. The dependence of resolution upon bandwidth B_i is shown in Fig. 3. The resolution in the traditional GI setup as a function of the lower bound is represented by the blue line at the top of Fig. 3(a). In FGI the resolutions initially decrease rapidly and then level off to a stable value with the increase of the lower bound T_i $(i = 1,2)$ when the filter bandwidths B_i $(i = 1,2)$ are taken to be equal for both filters and given the values of $B_i = 1$, 3, and 5. It is obvious that all the resolutions in FGI are much better compared with GI. It is also found that the resolution can be improved by decreasing the bandwidths B_i $(i = 1,2)$ for given T_i $(i = 1,2)$, as shown in Fig. 3(b), where we have taken T_i $(i = 1,2) = 5$, 15, and 25. From these results we can set suitable bandwidth conditions for performing the following imaging experiments. It is worthy to note that the best resolution can be as small as the size of one pixel of CCD2, and even seems to be slightly smaller than this in Fig. 3(b). However, this is caused by numerical approximations in data processing, and physically we should surmise that the resolution is limited to one pixel for both low-pass and high-pass filtering.

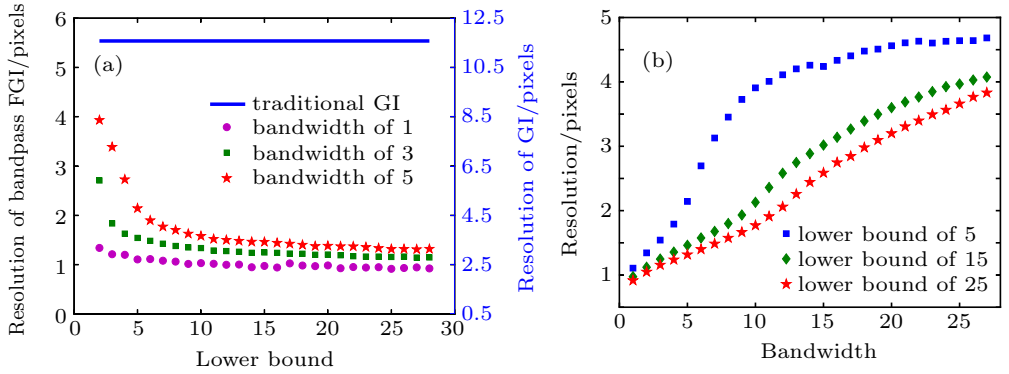


Fig. 3. Relationships between resolution and bandwidth. The blue line represents the resolution of GI, and dots represent that of FGI. (a) Resolution vs. lower bound T_i $(i = 1,2)$ of the filter bandwidths for different given bandwidths of B_i $(i = 1,2) = 1$, 3, and 5. (b) Resolution vs. bandwidth B_i $(i = 1,2)$ for different given lower bounds of T_i $(i = 1,2) = 5$, 15, and 25.

Unfortunately, to date we have no good physical explanation for this, and can only provide a simple heuristic explanation. We may consider the correlation values $g^{(2)}(x_1,x_2)$ and $g_B^{(2)}(x_1,x_2)$ for the following three different cases.

1) When $x_1 = x_2$, the intensity values of both $I(x_1)$ and $I(x_2)$ have completely identical fluctuations and so $I_{B1}(x_1)$ and $I_{B2}(x_2)$ are also the same after being filtered. Though some data have been simultaneously removed from both beams, the remaining values are still correlated. Therefore, it is possible for $g_B^{(2)}$ to have almost the same value as $g^{(2)}$.

2) When $x_1 \neq x_2$ but $|x_1 - x_2|$ is less than the coherence length, the intensities of $I(x_1)$ and $I(x_2)$ are partially correlated and have different instantaneous values, so that when some values are removed, $I_{B1}(x_1)$ and $I_{B2}(x_2)$ are not completely identical, i.e., they are not synchronous, which means that $I_{B1}(x_1)$ will be equal to 0 at certain times due to filtering while $I_{B2}(x_2)$ will have non-zero values at the same time, and vice versa. This is different from case 1, so that $\langle I_{B1}(x_1) I_{B2}(x_2)\rangle$ will be $\leq \langle I(x_1) I(x_2)\rangle$. The larger $|x_1 - x_2|$ is, the more pronounced this will be, and $\langle I_{B1}(x_1) I_{B2}(x_2)\rangle$ will become much smaller than $\langle I(x_1) I(x_2)\rangle$ when the bandwidth value is chosen to be very small. Though $\langle I_{B1}(x_1)\rangle \langle I_{B2}(x_2)\rangle$ is also smaller compared with $\langle I(x_1)\rangle \langle I(x_2)\rangle$ after filtering, it is possible for $g_B^{(2)}$ to be smaller than $g^{(2)}$. This applies to all the other positions within the transverse coherence length. When the values of $g_B^{(2)}$ at these positions are smaller than those of $g^{(2)}$, this will make the FWHM of $g_B^{(2)}$ narrower, leading to super-resolution.

3) When $x_1 \neq x_2$ and both are outside the coherence length, both $g^{(2)}$ and $g_B^{(2)}$ are equal to 1 since $I(x_1)(I_{B1}(x_1))$ and $I(x_2)(I_{B2}(x_2))$ are completely uncorrelated.

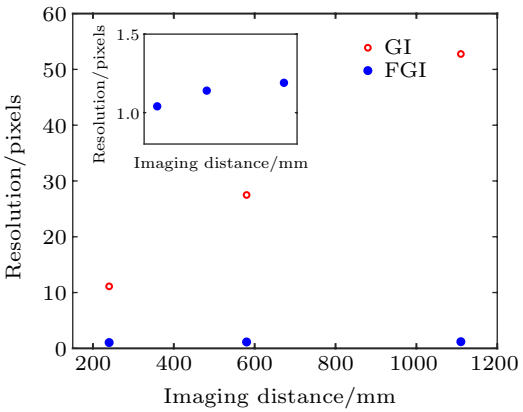


Fig. 4. Resolution vs. imaging distance in GI and bandpass FGI. Inset: FGI resolution on an amplified scale.

Though the discussion above is not a rigorous theoretical deduction, it is a direct intuitive explanation of why bandpass FGI can produce a super-resolution image. It is well-known that the intensity of a thermal field has negative exponential statistics. For the same bandwidth, the more extreme the lower/upper bound of the bandwidth, the more often will the value of 0 appear in the filtered intensity, which will

improve the resolution compared with the case of a smaller lower/upper bound, as shown in Fig. 3(a). This is why the resolution strongly depends on the bandwidth and its lower/upper bound.

According to the well-known relation $\Delta x \propto \lambda z/D$, where Δx is the spatial resolution of a traditional GI system, with a constant light source of size D and wavelength λ we first performed spatial HBT experiments to compare the different resolutions Δx of GI and FGI by changing the imaging distance z. As shown in Fig. 4, the resolution of GI (red circles) worsens with increasing distance, as expected. However, though the resolution also deteriorates a little due to inevitable experimental errors after bandpass filtering with a bandwidth of 1 (blue dots), its value can be improved by a factor of more than 10, 23, and 42 at distances of 240 mm, 580 mm, and 1110 mm, respectively. The inset of Fig. 4 shows the FGI resolutions at different distances on an amplified scale, from which we can see that the best resolutions are very close to the size of one pixel. The enhancement factor can be further increased by designing the FGI system with longer imaging distances or a smaller light source. However, it should be recognized that no matter how large this factor is, the absolute resolution can never be smaller than the size of a pixel. Even so, FGI can play an important role in the field of super-resolution imaging of macroscopic objects such as in remote sensing.

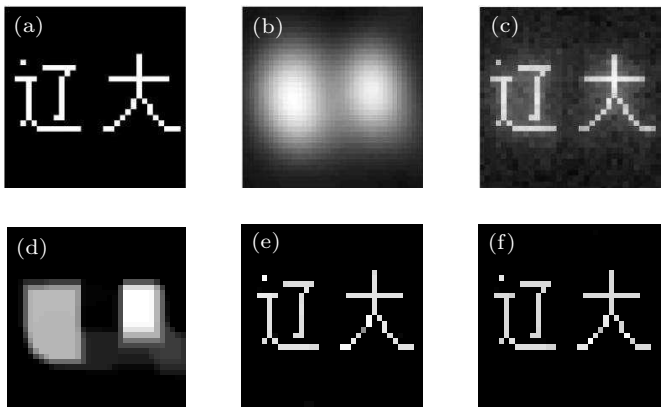


Fig. 5. (a) Digital binary object. (b) Reconstructed traditional GI image with 50000 exposures. (c) Reconstructed FGI image with 50000 exposures. (d) Reconstructed GI image using CS with 2000 exposures. (e) and (f), Reconstructed FGI images using CS with 400 and 500 exposures, respectively.

To verify our method, a digital binary object[35] of size 64×64 pixels was first used to simulate traditional GI and band-pass FGI in an autocorrelation scheme. The simulated object was a transmission mask, consisting of two Chinese characters representing a shortened form of Liaoning University, as shown in Fig. 5(a); it is assumed that this is inserted into the test beam very close to CCD1. The bucket signals for conventional GI and bandpass FGI are obtained by convoluting the intensities $I(x_1)$ and $I_{B1}(x_1)$, respectively, with the digital object and then summing over all the pixels. The values $B_1 = B_2 = 3$ and $T_1 = T_2 = 51$ were set to obtain the filtered intensity distributions. For a sampling number of 50000, the results are shown in the first row of Fig. 5, where the images $g^{(2)}(x_2)$ and $g_B^{(2)}(x_2)$ retrieved from Eqs. (2) and (4) are shown in Figs. 5(b) and 5(c), respectively. It is evident that the two characters in the traditional GI image are completely blurred, while in the image reconstructed by bandpass FGI they are clearly distinguishable with excellent image quality. The experiment was then repeated but using CS processing, and the results are shown in the second row of Fig. 5. Figure 5(d) was retrieved by CS GI with 2000 exposures, while figures 5(e) and 5(f) were reconstructed by CS FGI with just 400 and 500 samplings, respectively. It can be seen in Fig. 5(d) that even though CS was applied, the GI image is indecipherable, while FGI combined with CS can achieve excellent resolution with a sampling number much smaller than the Nyquist limit of $64 \times 64 = 4096$ in our case.

4. Conclusions

We have performed FGI experiments with and without using CS to achieve super-resolution images based on our bandpass filtering scheme. It is found that the resolution can be improved by more than an order of magnitude compared with the Rayleigh diffraction limit of a GI system, and can be further enhanced through optimization of the optical setup. It has also been shown (in Fig. 5) that FGI plays the key role in the improvement of resolution and not CS, which of course has its other benefits. However, FGI together with CS combines the advantages of both techniques, and offers a new route to realize super-resolution GI with better image quality but many fewer exposures (about 10% of the Nyquist limit). It should be noted, however, that the actual ultimate resolution will be limited by the pixel size of the reference detector CCD2 due to data post-processing. Nevertheless, if a field such as filtered thermal light could be generated directly in a computational GI scheme, the resolution would then not be limited by the pixel size of the reference detector, and could be reduced to dozens of nanometers. Therefore, FGI combined with CS should be an important potential candidate in the field of super-resolution imaging for not only remote sensing but also microscopy.

References

[1] Born M and Wolf E 1999 *Principles of Optics: Electromagnetic Theory of Propagation, Interference and Diffraction of Light* (New York: Cambridge University Press)
[2] Hell S W 2007 *Science* **316** 1153
[3] Betzig E, Patterson G H, Sougrat R, Lindwasser O W, Olenych S, Bonifacino J S, Davidson M W, Lippincott-Schwartz J and Hess H F 2006 *Science* **313** 1642
[4] Moerner W E 2007 *Proc. Natl. Acad. Sci. USA* **104** 12596
[5] Pittman T, Shih Y H, Strekalov D and Sergienko A 1995 *Phys. Rev. A* **52** R3429

[6] Cheng J and Han S S 2004 *Phys. Rev. Lett.* **92** 093903
[7] Gatti A, Brambilla E, Bache M and Lugiato L A 2004 *Phys. Rev. Lett.* **93** 093602
[8] Ferri F, Magatti D, Gatti A, Bache M, Brambilla E and Lugiato L A 2005 *Phys. Rev. Lett.* **94** 183602
[9] Cai Y J and Zhu S Y 2005 *Phys. Rev. E* **71** 056607
[10] Cao D Z, Xiong J and Wang K G 2005 *Phys. Rev. A* **71** 013801
[11] Valencia A, Scarcelli G, D'Angelo M and Shih Y 2005 *Phys. Rev. Lett.* **94** 063601
[12] Zhang D, Zhai Y H, Wu L A and Chen X H 2005 *Opt. Lett.* **30** 2354
[13] Chen X H, Liu Q, Luo K H and Wu L A 2009 *Opt. Lett.* **34** 695
[14] Zhang P L, Gong W L, Shen X, Huang D J and Han S S 2009 *Opt. Lett.* **34** 1222
[15] Sprigg J, Peng T and Shih Y H 2016 *Sci. Rep.* **6** 38077
[16] Gong W L and Han S S 2012 *Phys. Lett. A* **376** 1519
[17] Oh J E, Cho Y W, Scarcelli G and Kim Y H 2013 *Opt. Lett.* **38** 682
[18] Yao X R, Li L Z, Liu X F, Yu W K and Zhai G J 2015 *Chin. Phys. B* **24** 044203
[19] Chen X H, Kong F H, Fu Q, Meng S Y and Wu L A 2017 *Opt. Lett.* **42** 5290
[20] Meng S Y, Sha Y H, Fu Q, Bao Q Q, Shi W W, Li G D, Chen X H and Wu L A 2018 *Opt. Lett.* **43** 4759
[21] Cao D Z, Xiong J, Zhang S H, Lin L F, Gao L and Wang K G 2008 *Appl. Phys. Lett.* **92** 201102
[22] Chan K W C, O'Sullivan M N and Boyd R W 2009 *Opt. Lett.* **34** 3343
[23] Chen X H, Agafonov I N, Luo K H, Liu Q, Xian R, Chekhova M V and Wu L A 2010 *Opt. Lett.* **35** 1166
[24] Ferri F, Magatti D, Lugiato L A and Gatti A 2010 *Phys. Rev. Lett.* **104** 253603
[25] Shapiro J H 2008 *Phys. Rev. A* **78** 061802(R)
[26] Luo K H, Huang B Q, Zheng W M and Wu L A 2012 *Chin. Phys. Lett.* **29** 074216
[27] Katz O, Bromberg Y and Silberberg Y 2009 *Appl. Phys. Lett.* **95** 131110
[28] Shechtman Y, Gazit S, Szameit A, Eldar Y C and Segev M 2010 *Opt. Lett.* **35** 1148
[29] McKechnie T S 1972 *Opt. Acta* **19** 729
[30] Chmyrow A, Keller J, Grotjohann T, Ratz M, d'Este E, Jakobs S, Eggeling C and Hell S W 2013 *Nat. Methods* **10** 737
[31] Yu W T, Ji Z H, Dong D S, Yang X S, Xiao Y F, Gong Q H, Xi P and Shi K B 2016 *Laser Photon. Rev.* **10** 147
[32] Chen Z P, Shi J H and Zeng G H 2016 *Appl. Opt.* **55** 8644
[33] Wright S J, Nowak R D and Figueiredo M A T 2009 *IEEE Trans. Signal Process* **57** 2479
[34] Zhao C Q, Cong W L, Chen M L, Li E R, Wang H, Xu W D and Han S S 2012 *Appl. Phys. Lett.* **101** 141123
[35] Basano L and Ottonello P 2007 *Opt. Express* **15** 12386